Journal of Nano- and Electronic Physics
Vol. **13** No 2, 02013(4pp) (2021)

Журнал нано- та електронної фізики
Том **13** № 2, 02013(4cc) (2021)

Electrical Properties and Magnetic Field Dependent *I-V* Characteristics of Nanocrystalline Cobalt Doped Nickel Ferrite

P. Ghosh, P. Mitra*

Department of Physics, The University of Burdwan, West Bengal, India

(Received 11 January 2021; revised manuscript received 25 March 2021; published online 09 April 2021)

The influences of cobalt doping in nickel ferrite on electrical conductivity, dielectric properties (measured over a wide frequency range of 42 Hz to 5 MHz) and magnetic field (up to 15 kOe) dependent *I-V* characteristics are measured. Information about magneto resistance is very much necessary for magnetic property dependent electrical application of chemical routed $Co_xNi_{1-x}Fe_2O_4$. Material was prepared by sol gel self combustion technique. Characterization of synthesized powders were made using X-ray diffraction (XRD) with Rietveld fitting.

Keywords: Magnetoresistance, XRD, Rietveld fitting.

DOI: 10.21272/jnep.13(2).02013 PACS numbers: 72.25. – b, 78.70.Ck

1. INTRODUCTION

Potential applications of ferrites draw considerable scientific and technological interest from past decades to the present days. Ferrite is a ceramic material which is electrically non conductive and magnetically ferrimagnetic [1-3] material. On the basis of structure many ferrites adopt the spinel structure with the formula AB_2O_4, where A and B represents metallic cations including iron. Like other ferrites, spinel ferrites are classified as soft, semi hard or hard based on their resistance to be demagnetized. $Mn_aZn_{1-a}Fe_2O_4$, $Ni_aZn_{1-a}Fe_2O_4$ are well known soft ferrites and $CoOFe_2O_3$ is classified as semi hard ferrite [4-6]. Soft ferrites possess low coercivity hence low hysteresis loss while the materials have high resistivity that prevents eddy current, another source of energy loss. For the low losses at high frequency they are used in cores of RF transformers, switch mode power suppliers, loopstick antennas in AM radios and in various microwave components [7-9]. Semi hard magnetic materials are used for its magnetostrictive applications like sensors and actuators. Hard magnetic materials are used for permanent magnet applications, medium for magnetic recording, bio diagnostics purposes etc. [10]. Nickel ferrite and cobalt ferrite both possess inverse spinel structure at bulk state. For these materials, cation distribution is characterized by the inversion parameter i.e. the fraction of divalent ions present in the octahedral sites. Unit cell geometry controlled by the metal oxygen bond lengths for tetrahedral and octahedral sites. Cobalt nickel ferrite is considered to be important for the present days for various applications for it controlled electrical conductivity as well as good magnetic response.

2. MATERIALS AND METHODS

The nanoparticles of $Co_xNi_{1-x}Fe_2O_4$ ferrite were synthesized by using sol-gel-auto-combustion method. Cobalt nitrate hexahydrate $[Co(NO_3)_2{\cdot}6H_2O]$, nickel nitrate hexahydrate $[Ni(NO_3)_2{\cdot}6H_2O]$ and iron (III) nitrate nonahydrate $[Fe(NO_3)_3{\cdot}9H_2O]$ dissolved in distilled water according to the desired molar proportion. Then polyvinyl alcohol (PVA) was added to it under constant stirring to transform the solution into a colloidal solution. Drop wise addition of (NH_4OH) (25 % concentration) leads to the formation of a sol of metal hydroxides. It was subsequently dried at 100 °C for 12 h. The dried gel was ignited in a corner on a heated surface and an exothermic reaction takes place at ~250 °C. Finally pellets were formed from the powder and get heat treated at 600 °C for 2 h.

X-ray diffraction (XRD) patterns of samples have been taken by employing a Bruker (D8 advance) X-ray diffractometer with Ni-filtered CuK_α radiation (with $\lambda = 1.5418$ Å). Electrical impedance spectra were recorded using impedance analyzer (Model-Hioki 353250). The *I-V* characteristics were measured using Keithley dual source Meter (Model: 2410-C) where sample was placed in the pole gap of an electromagnet (MicroSense, USA) using a sample holder of Pt electrodes. Proper contact between sample surface and electrode surface was made by adjusting the pressure from both sides. DC voltage was applied to the Pt electrodes by connecting it with Keithley Meter. *I-V* measurement was done in the presence and absence of dc magnetic field (up to 15 kOe) and voltage was swept with sequence up (0 → ± 50 V) and down (0 → ± 50 V) modes. The direction of the magnetic field perpendicular to the disc is considered as positive and then opposite to the initial direction is taken as negative. The influence of magnetic field (H) on the *I-V* curves was recorded in the presence of selected magnetic fields in two segments, i.e. first segment (E_1): increase of H in positive direction, second segment (E_2): increase of H in negative direction. We repeated the experiment for voltage up and voltage down modes. The hysteresis nature of the *I-V* curves was recorded by completing the bias voltage cycling (0 V → + 50 V → 0 V → – 50 V→ 0 V). Hysteresis loop Irreversibility feature) was measured in the presence and absence of magnetic field to gather the information

* mitrapartha1@rediffmail.com
The results were presented at the International Conference on Multifunctional Nanomaterials (ICMN2020)

how magnitude and direction of magnetic field affected the loop nature. The delay time between two consecutive voltage points was set to 100 ms. No waiting time (t_w) was given between the application of magnetic field and starting the measurement of *I-V* characteristics.

3. RESULTS AND DISCUSSION

3.1 XRD Analysis

Fig. 1 shows the X-ray diffraction pattern of $Co_xNi_{1-x}Fe_2O_4$ [$x = 0$, 0.2, 0.4, 0.6] powders. First XRD at the bottom of Fig. 1 is for pure nickel ferrite. For this material diffraction peaks are observed at 30.41°, 35.84°, 37.47°, 43.60°, 53.79°, 57.77°, 63.45°, 72.05° and 75.11° respectively [JCPDS file No. 44-1485]. The corresponding crystallographic planes are (220), (311), (222), (400), (422), (511), (440), (620) and (533) respectively. The XRD patterns reveals the peaks are in good agreement with face centered cubic spinel structure. As no other peak is present there, hence single and pure phase of the material is confirmed. Rietveld fitting has been done using Maud software. The Rietveld fitting outputs are shown in Fig. 2 for the sample $x = 0.2$ and $x = 0.6$. The difference plot i.e. the residual of fitting ($I_0 - I_c$) between the observed pattern (I_0) and fitted pattern (I_c) is shown at the bottom of Fig. 2 below the respective patterns. Lattice parameter increases with cobalt incorporation. Lattice parameters are 8.324 Å, 8.336 Å, 8.353 Å, 8.366 Å for $x = 0$, $x = 0.2$, $x = 0.4$, $x = 0.6$ samples, respectively. The average value of particle size decreases with increment of x value. For pure nickel ferrite, particle size estimated from Rietveld refinement using MAUD software is ~ 137.8 nm and these value decreases up to 94.6 nm for $x = 0.6$ sample. The intensity of almost all the diffraction peaks decreases with larger value of x and slight broadening of diffraction peaks for larger x value sample clearly indicates lowering of particle size.

Appropriate fitting is indicated by the continuous line of fit. GoF's for all the cases are lying under 1.4 that indicates fitting equations are suitable enough for the experimental data. The goodness factor is defined as the ratio weighted residual error and expected error.

As cobalt ferrite and nickel ferrite both are inverse spinel hence nickel and cobalt ions occupy octahedral B sites. When mixed cobalt nickel ferrite samples are synthesized by sol gel combustion technique, the lattice parameter increases with cobalt incorporation, which is due to replacement of smaller Ni^{2+} ions (0.069 nm) by larger Co^{2+} ions (0.074 nm) as per Vegard's law, confirmed from Rietveld refinement data.

3.2 Impedance Spectroscopy

Complex impedance plots (Nyquist plots) for sample $x = 0.4$ and $x = 0.6$ help to investigate the ionic transport property with the proper understanding of the grain and grain boundary resistances of the material. Complex impedance $Z^*(\omega)$ is expressed by the equation

$$Z^*(\omega) = Z'(\omega) - Z''(\omega). \quad (1)$$

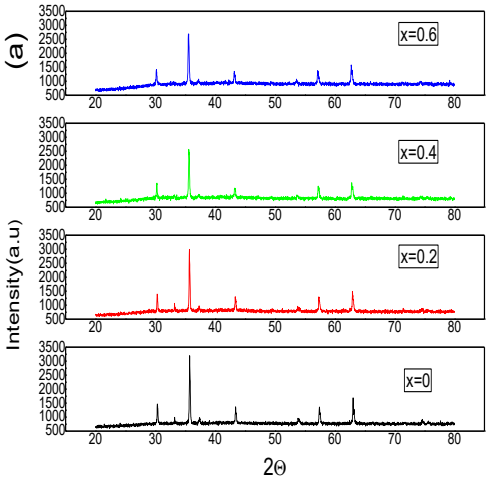

Fig. 1 – X-ray power diffraction patterns of $Co_xNi_{1-x}Fe_2O_4$ for $x = 0$, $x = 0.2$, $x = 0.4$ and $x = 0.6$

Fig. 4a, b represent the Nyquist plots for $x = 0.4$ and $x = 0.6$ samples respectively at different temperatures varying from 200 °C to 260 °C. The Nyquist plot is characterized by the presence of depressed and broad semi-circular arcs at each temperature and it generally indicates the presence of non-Debye type relaxation process. It is observed that the radius of the broad semi-circular arc decreases with increase in temperature, indicating increase in conductivity attributed to lowering of barrier and subsequent increase of the mobility of charge carriers. The values of $C_{gb} = 21.42$ pF, $R_{gb} = 41.2$ MΩ, $C_g = 18.89$ pF, $R_g = 16$ MΩ for $x = 0.4$ sample (at 200 °C) change to $C_{gb} = 41.22$ pF, $R_{gb} = 17.8$ MΩ, $C_g = 71.65$ pF, $R_g = 11.7$ MΩ for $x = 0.6$ sample (at 200 °C).

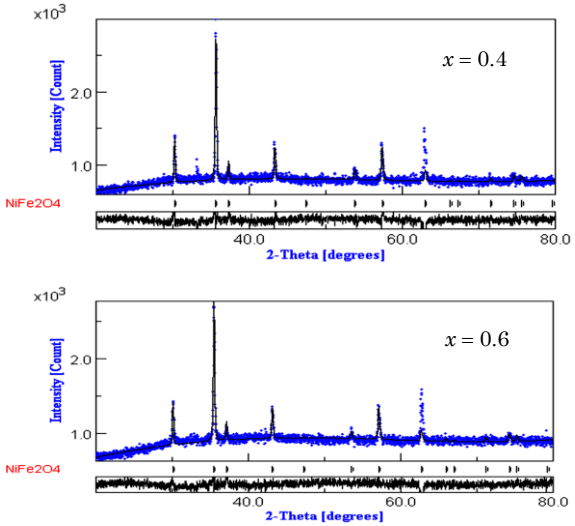

Fig. 2 – Fitted X-ray powder diffraction patterns for $x = 0.4$ and $x = 0.6$ samples respectively with the residual of fitting at the end of each fitting

Thermally activated process is solely responsible for the conduction in bulk and grain boundary region as like as the semiconducting materials. The depressed circular nature of the plots suggest an equivalent circuit which is a series combination of two resistors (R_b, R_{gb}) parallel with constant phase elements (Q_b, Q_{gb})

corresponding to bulk and grain boundary contribution of the material. EC-Lab software was used to fit the Nyquist plots using the equivalent circuit model. The values of capacitance (C) from the modified capacitive phase element (Q) for bulk (grain) as well as grain boundary are calculated using expression [25]:

$$C = R^{\frac{1-a}{a}} Q^{\frac{1}{a}}. \qquad (2)$$

The values of resistances (R) corresponding to bulk and grain boundary for all samples decreases with the increase of temperature while the value of capacitance (C) decreases. The samples are identified with higher grain boundary resistances than the grain interior resistances. Exactly opposite phenomena are observed for the capacitances. The value of the exponent (a) for all the cases lies between 0.85 to 0.98. The value of exponent which is smaller than 1 confirms the presence of non-Debye type relaxation for different grain size of the sample. When we compare between two samples of different grain size then it is clearly expressed from the graph that bulk resistance as well as grain boundary resistance decreases with cobalt incorporation.

As the bulk resistance and grain boundary resistance both decrease with temperature hence total conductivity of the material become an increasing function of temperature which follows the relation

$$\sigma_{tot} = \sigma_{dc}(T) + \sigma(\omega, T) = \sigma_{dc}(T) + \sigma(T)\omega^n. \qquad (3)$$

Here, $\sigma_{dc}(T)$ is the dc limit of ac conductivity, arises due to thermally activated transitions of electron from valance band to conduction band and creation of hole in valance band. The $\sigma(\omega, T)$ is the frequency activated (AC) conductivity due to hopping process among ions of the same element in more than one valence state. Here $\alpha(T)$ is temperature dependent constant and n represents the degrees of coupling between the charge carriers and ions present in the neighboring sites while performing hopping. Fig. 3 represents the plots of total conductivity against frequency for the sample $x = 0.4$ and $x = 0.6$ respectively. At low frequency region, the dc limit of ac conductivity (σ_{dc}) can be taken as a contribution from grain boundaries. At high frequency region, the conductivity rapidly increases with frequency. This is due to electronic hopping between Fe^{2+} and Fe^{3+} ion pairs in the octahedral (B) sites. The temperature variation of the exponent 'n' is generally used to gather information on the nature of charge transport through polaron hopping mechanism. In spinel ferrite total charge distribution is polarized via coulomb attraction between the moving electron and the surrounding electronic core structure present in the lattices. This leads to formation of phonon assisted polaron.

3.3 Magnetic Field Dependent Current-Voltage (*I-V*) Characteristics

Fig. 4c, d highlight the hysteresis nature of *I-V* curves in presence of magnetic field + 15 kOe which are measured by completing the bias voltage cycling (0 V → + 50 V → 0 V → – 50 V → 0 V). Fig. 4c shows the *I-V* loops for $x = 0.4$ sample, while Fig. 4d represents the *I-V* loops for $x = 0.6$ sample.

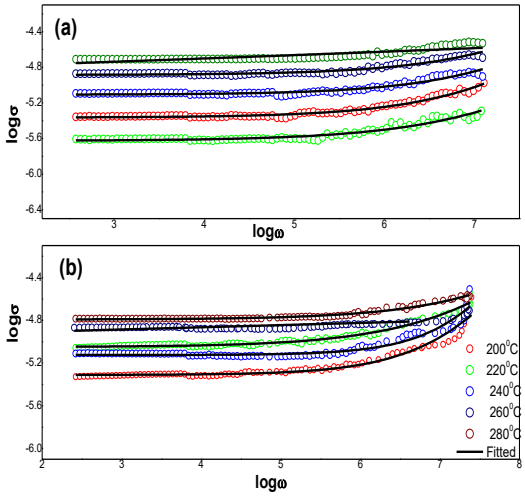

Fig. 3 – Frequency dependence of conductivity at selected temperatures for (a) $x = 0.4$ and (b) $x = 0.6$ samples

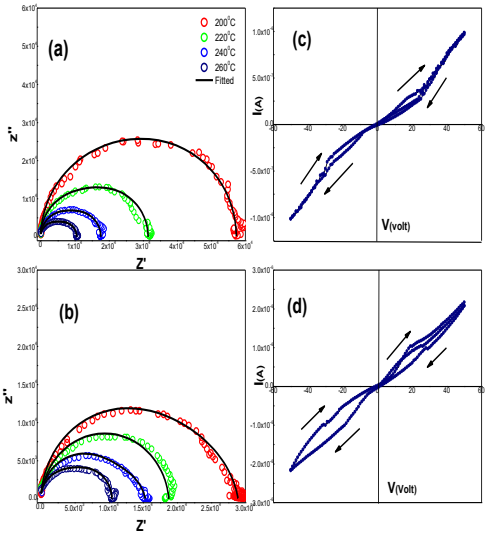

Fig. 4 – Nyquist plots for (a) $x = 0.4$ and (b) $x = 0.6$ samples at different temperatures. *I-V* loops in presence of + 15 kOe magnetic field for (c) $x = 0.4$ and (d) $x = 0.6$

The *I-V* curves are highly irreversible upon reversing the direction of up and down modes of bias voltage, irrespective of the positive and negative bias modes. Area under the *I-V* loops depend on cobalt incorporation within the material. Generally, loop area (representing electrical energy loss) is relatively small in the absence of magnetic field and it opens up in the presence of magnetic field in case of all the samples. The increase of loop area for magnetic field suggests the increase of electron scattering effect and it leads to more loss of electrical energy. Bi-stable electronic states that present in the samples (low resistance state (LRS) during voltage up mode and high resistive state (HRS) during voltage down mode) are clarified from these graphs.

Fig. 5 shows the *I-V* curves for $x = 0.4$ and $x = 0.6$ samples respectively with biasing voltage (0 → + 50 V and 0 → – 50 V) in the presence of selected magnetic fields (5, 10, 12, and 15 kOe). The current increases almost linearly up to a certain voltage (~ 15 V) and nonlinear nature becomes more prominent at higher

biasing voltage. The nature of *I-V* curves at forward bias and reverse bias, measured in the presence of magnetic field, is not identical. However, the *I-V* curves showed some noticeable changes in the features. First, one is the immediate enhancement of current magnitude, which gradually decreases with the further increase of magnetic field. Second, one is that non-linear character of the *I-V* curves at higher biasing voltage with distinct peak like feature appears in the *I-V* curves at forward biasing mode. The typical feature of decreasing current with the increase of the magnitude of bias voltage is called the negative differential resistance (NDR) effect in the *I-V* characteristics of the material. The nature of *I-V* curves for positive (forward) and negative (reverse) bias may sometimes be affected by the goodness of electrical contacts at both sides of the disc shaped sample. However, the basic features of the *I-V* curves are not significantly altered in our measurement in the presence of negative magnetic fields, although some irreversible effects are observed in the *I-V* curves. In both cases, NDR effect appeared at forward bias mode and in the presence of magnetic field. This is a clear evidence of magnetic field induced electronic property in the system. Looking a nearly linear variation of the *I-V* characteristics at lower biasing voltages, we attempted to fit the data by applying the child's law: $I(V) \sim V^m$, using space charge limited current (SCLC) mechanism. The power factor (m) was obtained from the slope of the linear extrapolation of the $\frac{\partial \ln I}{\partial \ln V}$ vs. V plot. This is consistent with the decrease of current magnitude with the increase of magnetic field, where magnetic field increases electron scattering effect in the current conduction path.

In a solid material where SCLC mechanism dominates, the *I-V* curve is expected to exhibit a sharp increase with voltage according to the m value.

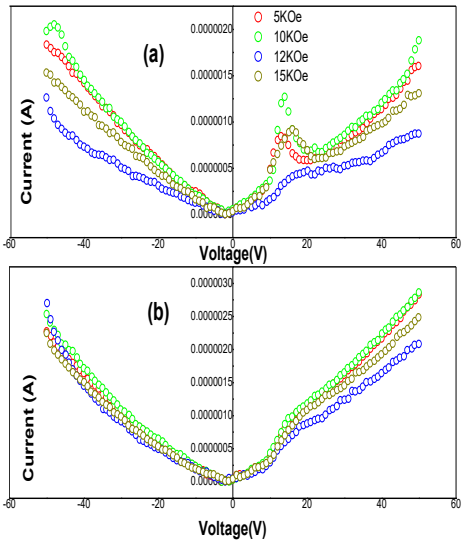

Fig. 5 – *I-V* curves in presence of selected magnetic fields without waiting time for (a) $x = 0.4$ and (b) $x = 0.6$ samples

4. CONCLUSIONS

For the nanocrystalline cobalt nickel ferrite samples synthesized by sol gel combustion technique, the lattice parameter increases with cobalt incorporation, which is due to replacement of smaller Ni^{2+} ions (0.069 nm) by larger Co^{2+} ions (0.074 nm) as per Vegard's law. Materials become less resistive with cobalt incorporation confirmed from both impedance spectra and *I-V* curves. The difference between LRS and HRS of *I-V* loop increases with cobalt substitution which manifests its importance for electronic memory based devices. Magnetic field dependent *I-V* curves are very much helpful to extract information about magnetoresistance (MR) of such type of materials.

REFERENCES

1. M. Hofmann, S.J. Campbell, H. Ehrhardt, R.J. Feyerherm, *J. Mater. Sci.* **39**, 5057 (2004).
2. A. Sutka, G. Mezinskis, G. Strikis, A. Siskin, *Energetika* **58**, 166 (2012).
3. M. Siddique, N.M. Butt, *Physica B* **8**, 4211 (2010).
4. Zaka Ullah, Shahid Atiq, Shahzad Naseem, *J. Alloy. Compd.* **555**, 263 (2013).
5. N. Hosni, et al., *J. Alloy. Compd.* **694**, 1295 (2016).
6. A.G. Olabi, A. Grunwald, *Mater. Design* **29**, No 2, 469 (2008).
7. N.K. Prasad, A. Naulakha, N. Jha, S.S. Meena, D. Bahadur, O. Prakash, R.K. Mandal, *Int. J. Mater. Res.* **103**, 1 (2012).
8. K. Nejati, R. Zabihi, *Chem. Central J.* **6**, 23 (2012).
9. C.Y. Tsay, K.S. Liu, T.F. Lin, I.N. Lin, *J. Magn. Magn. Mater.* **209**, 189 (2000).
10. S.P. Gubin, Y.A. Koksharov, G.B. Khomutov, G.Yu. Yurkov, *Russ. Chem. Rev.* **74** No 6, 489 (2005).

Електричні властивості та залежні від магнітного поля вольт-амперні характеристики нанокристалічного феріту нікелю, легованого кобальтом

P. Ghosh, P. Mitra

Department of Physics, the University of Burdwan, West Bengal, India

Вивчається вплив легування кобальтом феріту нікелю на електропровідність, діелектричні властивості (вимірювані в широкому діапазоні частот від 42 Гц до 5 МГц) та залежні від магнітного поля (до 15 кОе) вольт-амперні характеристики. Інформація про магнітоопір дуже необхідна для залежних від магнітних властивостей електричних застосувань хімічного з'єднання $Co_xNi_{1-x}Fe_2O_4$. Матеріал готували методом золь-гелевого самозагоряння. Характеристика синтезованих порошків проводилася за допомогою рентгенівської дифракції (XRD) з підгонкою Рітвельда.

Ключові слова: Магнітоопір, XRD, Підгонка Рітвельда.